Detection of the density matrix through optical homodyne tomography without filtered back projection

G. M. D'Ariano*
Dipartimento di Fisica "Alessandro Volta", Università degli Studi di Pavia, Via A. Bassi 6, I-27100 Pavia, Italy and Istituto Nazionale di Fisica Nucleare, Sezione di Pavia, via A. Bassi 6, I-27100 Pavia, Italy

C. Macchiavello† and M. G. A. Paris‡
Dipartimento di Fisica "Alessandro Volta", Università degli Studi di Pavia, via A. Bassi 6, I-27100 Pavia, Italy
(Received 9 March 1994)

We propose an alternative method for detecting the density matrix of a radiation field via optical homodyne tomography. The method needs no assumption on the state, and the density matrix is recovered directly from averages on data. The tomographic reconstruction is very fast and provides very reliable statistics on line with detection. As a test of the method we present numerical results for a set of computer-simulated experiments, corresponding to different quantum states of the radiation source. Then a tomographic reconstruction is given for experimental data provided by Smithey *et al.* [Phys. Rev. Lett. **70**, 1244 (1993)].

PACS number(s): 42.50.Dv, 03.65.Bz, 42.65.Ky

In a recent paper Smithey *et al.* [1] developed a method for detecting the quantum mechanical state of the field via the so-called optical homodyne tomography. This opened new perspectives in providing complete experimental characterization of nonclassical states of radiation, making all information about the quantum source directly detectable [2].

A homodyne tomography of a single field mode a consists of an ensemble of repeated measurements of the quadratures $\hat{a}_\phi = \frac{1}{2}(ae^{-i\phi} + a^\dagger e^{i\phi})$ for various phases ϕ relative to the local oscillator of the homodyne detector. Smithey *et al.* reconstruct the density matrix via the Wigner function $W(\alpha,\bar{\alpha})$ of the field, namely, the quasiprobability for symmetrically ordered field operators. In this way their method needs a filtered backprojection of the Wigner function, setting the resolution with which $W(\alpha,\bar{\alpha})$ is determined. In some sense the coarse-graining cutoff corresponds to an *a priori* hypothesis on the detected state, and hence it may ultimately affect the result and the error statistics of the tomographic reconstruction (the cutoff should be tuned carefully as a function of the total number of measurements in the tomographic scanning). The purpose of this paper is to show that there is no need for backprojection filtering the data, whereas the density matrix can be directly recovered from averages on experimental data. This leads to an improved method of tomographic reconstruction of the density matrix, which greatly speeds up data analysis, and achieves very reliable error statistics on line with detection. Before presenting our method, here in the following we briefly recall the procedure of Ref. [1] for comparison.

From the probability distributions $p(x,\phi)$ of the outcomes x of $\hat{a}_\phi$, the Wigner function $W(\alpha,\bar{\alpha})$ is reconstructed through the formula [3]

$$W(\alpha,\bar{\alpha}) = \frac{1}{4\pi}\int_{-\infty}^{\infty} d\eta\,|\eta| \int_{-\infty}^{\infty} dx \int_0^{\pi} \phi\, p(x,\phi) \times \exp\left\{i\eta\left[x - \mathrm{Re}\left(\alpha e^{i\phi}\right)\right]\right\} . \quad (1)$$

The density matrix is then obtained using the Fourier transform

$$\langle x+x'|\hat{\rho}|x-x'\rangle = \int_{-\infty}^{\infty} dy\, e^{2ix'y} W(x+iy, x-iy) . \quad (2)$$

In the number representation the change of basis is expressed by the double integral

$$\langle n|\hat{\rho}|m\rangle \equiv \rho_{n,m} = \frac{1}{\sqrt{\pi 2^n 2^m n!m!}} \int_{-\infty}^{\infty} dx \int_{-\infty}^{\infty} dx' e^{-\frac{1}{2}(x^2+x'^2)} H_n(x) H_m(x')\, \langle x|\hat{\rho}|x'\rangle , \quad (3)$$

where $H_n(x)$ is the Hermite polynomial of degree n.

Notice that Eq. (1) allows evaluation of the Wigner function only when the probability density $p(x,\phi)$ is given in analytical form. In fact, any approximation of the average over $p(x,\phi)dxd\phi$ in terms of a finite sum over experimental data is meaningless, because the integral over η does not converge for any datum (x,ϕ). In order to make the method analytic, a smoothing procedure is required: in Ref. [1] this is accomplished by means of filtered backprojection techniques, which are standard in tomographic imaging [4].

*Electronic address: dariano@pv.infn.it
†Electronic address: macchiavello@pv.infn.it
‡Electronic address: paris@pv.infn.it

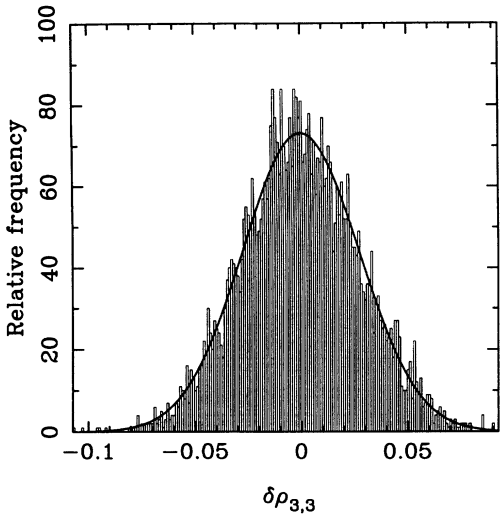

FIG. 1. Distribution of the tomographic outcomes for the matrix element $\rho_{3,3}$ (deviations $\delta\rho_{3,3}$ around the average). The computer-simulated experimental values are obtained for a coherent state with $\langle n\rangle = 3$. The histogram contains 5000 experiments (subensembles of data), each performed with $F = 27$ scanning phases and 100 measurements for each phase. The Gaussian curve with variance equal to the experimental rms error is superimposed.

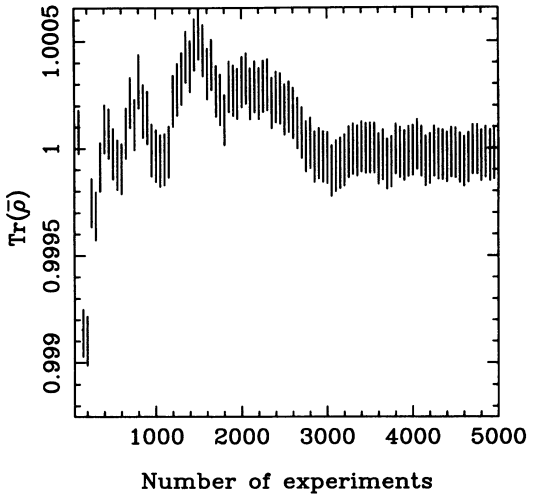

FIG. 2. Normalization of the density matrix versus number of experiments (subensembles of data) for a coherent state with $\langle n\rangle = 8$. Each experiment has been performed as in Fig. 1. The matrix is truncated at $n = 20$ photons.

Let us consider now a completely different procedure. The transformation (1) can be written more generally for any "s-ordering" quasiprobability distribution $W_s(\alpha,\bar{\alpha})$ [3]

$$W_s(\alpha,\bar{\alpha}) = \frac{1}{4\pi}\int_{-\infty}^{\infty} d\eta\,|\eta| \int_{-\infty}^{\infty} dx \int_0^{\pi} d\phi\, p(x,\phi) \times \exp\left\{\frac{1}{8}s\eta^2 + i\eta\left[x - \mathrm{Re}\left(\alpha e^{i\phi}\right)\right]\right\} . \quad (4)$$

For $s < 0$ the integral over η converges for any (x,ϕ), and thus commutes with the double integral over x,ϕ. This allows averaging on $p(x,\phi)$ in terms of statistical sums over finite sets of experimental data. For $s = -1$ the quasiprobability $W_{-1}(\alpha,\bar{\alpha})$ coincides with the Husimi Q function

$$Q(\alpha,\bar{\alpha}) \equiv \langle\alpha|\hat{\rho}|\alpha\rangle = W_{-1}(\alpha,\bar{\alpha}) , \quad (5)$$

which itself generates the matrix elements $\rho_{n,m}$ in the number representation according to the formula

$$\rho_{n,m} = \frac{1}{\sqrt{n!m!}}\frac{\partial^n}{\partial\bar{\alpha}^n}\frac{\partial^m}{\partial\alpha^m}\left(Q(\alpha,\bar{\alpha})\,\mathrm{e}^{|\alpha|^2}\right)\Big|_{\alpha=\bar{\alpha}=0} . \quad (6)$$

The derivatives in Eq. (6), with $Q(\alpha,\bar{\alpha})$ given by Eqs. (4) and (5), can be evaluated analytically. After a lengthy calculation one obtains

$$\rho_{n,n+d} = \sum_{m=0}^{\infty}\int_0^{\pi}\frac{d\phi}{\pi}\,\mathbf{R}^{(d)}_{nm}(\phi)\int_{-\infty}^{\infty} dx\, p(x,\phi)\, e^{-2x^2} x^{\langle d\rangle_2}\Phi\left(m-n-\frac{1}{2}d-\frac{1}{2}\langle d+1\rangle_2, \frac{1}{2}+\langle d\rangle_2; 2x^2\right) , \quad (7)$$

where $\mathbf{R}^{(d)}_{nm}(\phi)$ is the fixed matrix

$$\mathbf{R}^{(d)}_{nm}(\phi) = \left(2^{3/2}i\right)^{\langle d\rangle_2}\frac{2^{n+\frac{d}{2}+1}}{\sqrt{n!(n+d)!}}(-i)^{2n+d}\sum_{j_1=0}^{n}\sum_{j_2=0}^{d}(-1)^{j_2}\binom{n}{j_1}\binom{d}{j_2}(2n+d-2j_1-j_2)!(2j_1+j_2)!$$
$$\times\sum_{l_1=0}^{n-j_1+[\frac{d-j_2}{2}]}\sum_{l_2=0}^{j_1+[\frac{j_2}{2}]}\left(-\frac{1}{8}\right)^{l_1+l_2}\frac{(\cos\phi)^{2n+d-2j_1-j_2-2l_1}(\sin\phi)^{2j_1+j_2-2l_2}}{l_1!l_2!(2j_1+j_2-2l_2)!(2n+d-2j_1-j_2-2l_1)!}$$
$$\times\Gamma\left(n+\frac{1}{2}d-l_1-l_2+\frac{1}{2}\langle d\rangle_2+1\right)\,\delta(m-l_1-l_2) . \quad (8)$$

In Eq. (8), $\langle x\rangle_2$ denotes the rest of the division $x/2$, $[x]$ is the integer part of x, $\delta(n)$ is the Kronecker delta, and $\Phi(\alpha,\beta;z)$ is the confluent hypergeometric function of z with parameters α,β [5]. For F equally spaced phases $\phi_f = \frac{f\pi}{F}$

TABLE I. First few detected matrix elements of a squeezed state with $\langle n \rangle = 2$ and one squeezing photon (the matrix is real; the theoretical values are given in parentheses). The detected values are obtained for 120 experiments with $F = 27$ scanning phases and 120 measurements each.

	0	1	2	3	4	5
0	0.5279± 0.0013 (0.5275)	0.1538±0.0012 (0.1547)	0.2947±0.0015 (0.2957)	0.1396±0.0016 (0.1393)	0.2006±0.0019 (0.2015)	0.1133±0.0019 (0.1145)
1	0.1538±0.0012 (0.1547)	0.0432±0.0021 (0.0454)	0.0848±0.0014 (0.0867)	0.0418±0.0017 (0.0409)	0.0568±0.0016 (0.0591)	0.0336±0.0015 (0.0336)
2	0.2947±0.0015 (0.2957)	0.0848±0.0014 (0.0867)	0.1657±0.0021 (0.1658)	0.0799±0.0013 (0.0781)	0.1123±0.0016 (0.1130)	0.0666±0.0017 (0.0642)
3	0.1396±0.0016 (0.1393)	0.0418±0.0017 (0.0409)	0.0799±0.0013 (0.0781)	0.0387±0.0020 (0.0368)	0.0519±0.0014 (0.0532)	0.0313±0.0016 (0.0303)
4	0.2006±0.0019 (0.2015)	0.0568±0.0016 (0.0591)	0.1123±0.0016 (0.1130)	0.0519±0.0014 (0.0532)	0.0757±0.0022 (0.0770)	0.0440±0.0015 (0.0437)
5	0.1133±0.0019 (0.1145)	0.0336±0.0015 (0.0336)	0.0666±0.0017 (0.0642)	0.0313±0.0016 (0.0303)	0.0440±0.0015 (0.0437)	0.0271±0.0024 (0.0249)

$(f = 0, ..., F-1)$ the experimental mean value $\bar{\rho}_{n,n+d}$ of the matrix element $\rho_{n,n+d}$ is obtained from the following average:

$$\bar{\rho}_{n,n+d} = \sum_{m=0}^{[n+\frac{1}{2}d]} \frac{1}{F} \sum_{f=0}^{F-1} \mathbf{R}^{(d)}_{nm}(\phi_f) \left\langle e^{-2x^2} x^{\langle d \rangle_2} \Phi\left(m - n - \frac{1}{2}d - \frac{1}{2}(d+1)_2, \frac{1}{2} + \langle d \rangle_2; 2x^2\right) \right\rangle_{\phi_f} , \tag{9}$$

where $\langle \rangle_{\phi_f}$ denotes averaging over the subensemble of data for fixed phase $\phi = \phi_f$. Equation (9) is particularly suited to on-line data analysis; in fact, apart from the sum over data, the procedure requires just a single sum over m, whereas the hypergeometric functions $\Phi(\alpha, \beta; z)$ are connected to each other iteratively, and the matrix $\mathbf{R}^{(d)}_{nm}(\phi_f)$ is stored in the machine before beginning experiments.

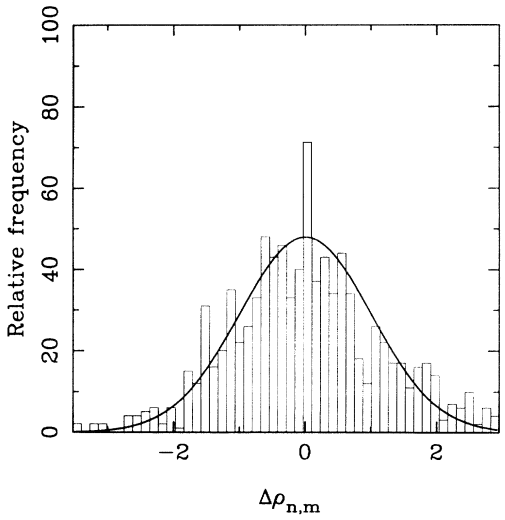

FIG. 3. Distribution of normalized deviations from the theoretical values $\Delta\rho_{n,m} \equiv (\bar{\rho}_{n,m} - \rho_{n,m})/\varepsilon_{n,m}$ for the first 30×30 matrix elements. The quantum state is a coherent one with $\langle n \rangle = 4$. The histogram pertains to 1000 experiments (subensembles of data) with $F = 27$ scanning phases each, and 200 measurements for each phase. A standardized (unit variance) Gaussian curve is superimposed.

We test our method on a set of Monte Carlo simulated experiments, with the aim of evaluating both the correctness of error statistics and the absence of systematic deviations from theoretical values.

In order to evaluate the statistical errors, we have preliminarily studied the distribution of the tomographic outcomes for each matrix element around its averaged value, checking that it is perfectly Gaussian for every matrix element, independent of the kind of considered quantum state. We have considered coherent, squeezed, and general quantum superpositions of number states (within this paper $F = 27$, with at least 100 measurements for each phase; the resolution $F = 27$ is used for comparison with Ref. [1], but one can get satisfactory results already for $F = 12$). Due to the normal distribution of deviations $\delta\rho_{n,m}$, the error $\varepsilon_{n,m}$ of the matrix element $\rho_{n,m}$ can be evaluated as usual, namely, by dividing the ensemble of data into subensembles (here also called "experiments"), and then calculating the rms deviation of the subensemble average with respect to the global average. In Fig. 1, we report a typical distribution of outcomes for a fixed matrix element, with the source in a coherent state: the agreement with the Gaussian probability is remarkable.

As regards the reliability of detection of the whole matrix, two significant tests have been performed: (i) the matrix normalization, and (ii) the χ^2 test. In Fig. 2, a sample of the normalization is given versus the number of data subensembles, for a highly excited coherent state (less excited states—coherent or not—exhibit a more rapid convergence). The distribution of normalized deviations from the theoretical values $\Delta\rho_{n,m} \equiv (\bar{\rho}_{n,m} - \rho_{n,m})/\varepsilon_{n,m}$ follows a standardized Gaussian curve. A sample histogram for the first 30×30 matrix elements is given in Fig. 3, for a coherent state with $\langle n \rangle = 4$. Notice that about 68% of the deviations

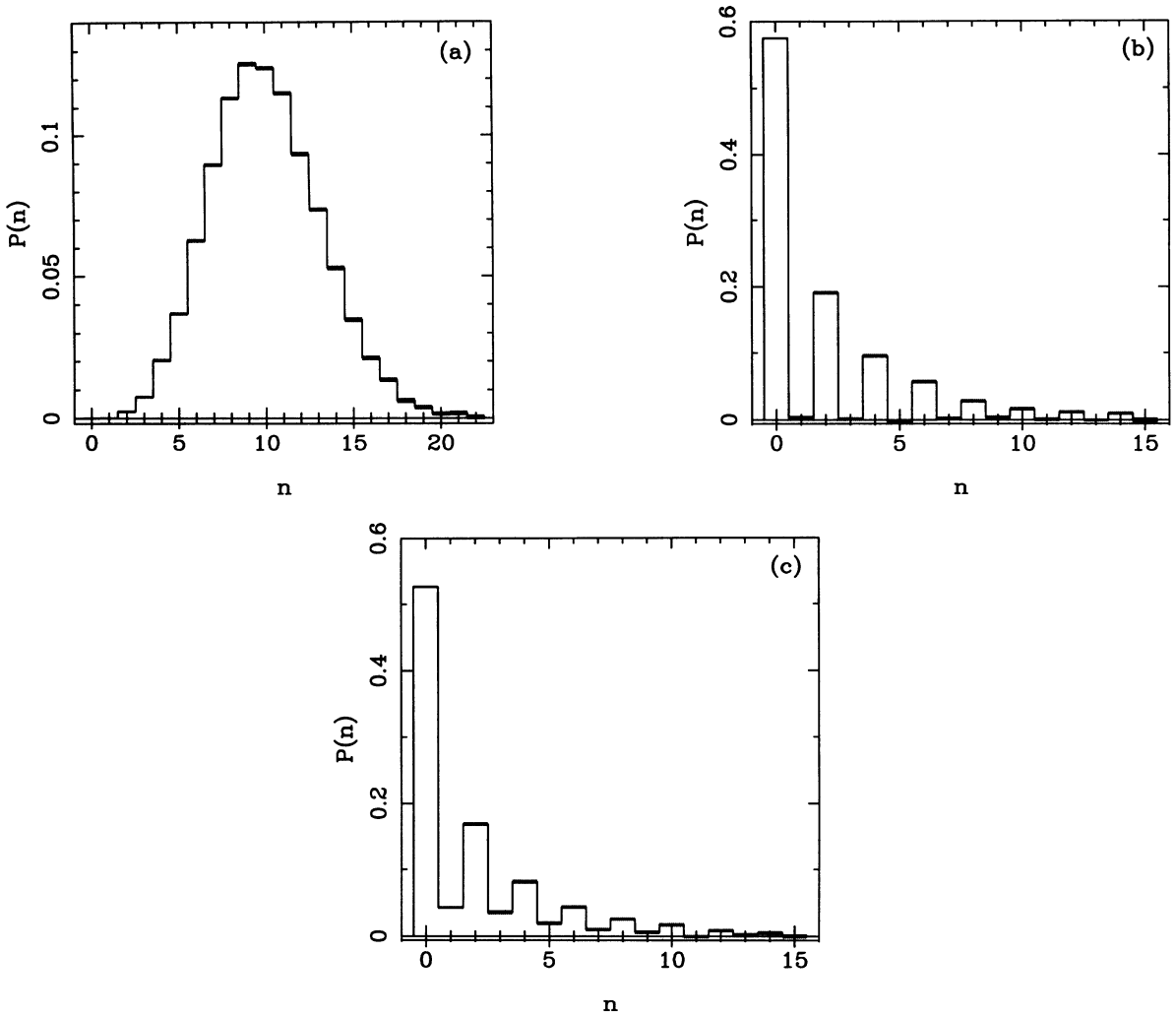

FIG. 4. Number probability distributions for various states (the thickness of horizontal lines corresponds to error bars). (a) Coherent state with $\langle n \rangle = 10$; (b) squeezed vacuum with $\langle n \rangle = 2$; (c) squeezed state with $\langle n \rangle = 2$ and 1 squeezing photon. [For all plots $F = 27$ scanning phases are used; there are 400 experiments (subensembles of data) and 300 measurements for each phase in plot (a), and 100 experiments and 100 measurements for each phase in plots (b) and (c).]

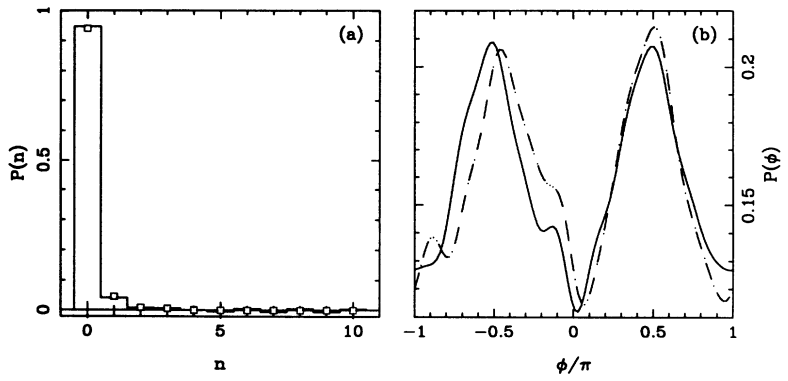

FIG. 5. Tomographic reconstruction from homodyne experimental data kindly provided by Beck and Raymer. Data have been grouped into 40 subensembles of 100 points for each of the $F = 27$ scanning phases. (a) Number probability distribution as in Fig. 4: the small squares correspond to evaluations provided by Beck and Raymer according to the original reconstruction method of Ref. [1]. (b) Ideal phase probability distribution: the full line is from the present method and the dashed line is from Beck and Raymer (see also Ref. [2]).

lie within one standard deviation, corresponding to an optimal χ^2 slightly greater than one. Analogous results have been obtained for all other kinds of states here considered.

We now present some Monte Carlo tests for different kinds of quantum states. In Table I the first few matrix elements are reported and compared with the theoretical values for a squeezed state with $\langle n \rangle = 2$ and one squeezing photon. The maximum index for the matrix elements is limited by both machine memory and precision (we compute matrix elements $\rho_{n,m}$ up to $n, m = 31$). In Fig. 4 we show the number probability distribution for a coherent state with $\langle n \rangle = 10$, and for two highly nonclassical states: a squeezed vacuum with two squeezing photons, and a squeezed state with $\langle n \rangle = 2$ and one squeezing photon. All plots reproduce theoretical values with great accuracy.

In Fig. 5, we compare our method with the original one [1] on the basis of a tomographic reconstruction from the same homodyne experimental data (kindly provided by Beck and Raymer). The quantum state is a weakly squeezed vacuum; due to nonunit quantum efficiency, the even-odd alternance in number probability is lost. The off-diagonal matrix elements here are synthetically represented by the resulting ideal phase distribution (for a recent review on phase detection see Ref. [6]). There is a qualitative agreement between the two methods; a precise quantitative comparison cannot be given, since error bars for the original reconstruction [1] are not available. However, a careful analysis shows that discrepancies larger than our estimated error bars are present, thus inferring that the original method either is affected by larger inaccuracy, or it suffers systematic errors due to filtering backprojection cutoff.

In conclusion, we have proposed an alternative method for detecting the density matrix of the radiation field via homodyne tomography. The method avoids filtered backprojection or any other smoothing procedure on experimental data, with no *a priori* assumption on the detected state. The density matrix is recovered from simple averages on data. The procedure allows very fast on-line data analysis, and leads to very reliable error statistics. A set of simulated experiments for various quantum states exhibit excellent quantitative agreement between theoretical and experimental matrix elements.

Without any doubt the tomographic detection represents a powerful tool for investigating quantum properties of radiation; we believe that with the present improved features—speed, precision, matrix dimension limits, and statistical reliability—this technique already can be used as a probe also for measuring internal parameters of quantum nonlinear optical devices, in other words, for experimentally characterizing effective quantum interaction Hamiltonians of optical media.

[1] D. T. Smithey, M. Beck, M. G. Raymer, and A. Faridani, Phys. Rev. Lett. **70**, 1244 (1993).

[2] The first applications of optical homodyne tomography are given in M. Beck, D. T. Smithey, and M. G. Raymer, Phys. Rev. A **48**, R890 (1993); D. T. Smithey, M. Beck, J. Cooper, and M. G. Raymer, *ibid.* **48**, 3159 (1993).

[3] K. Vogel and H. Risken, Phys. Rev. A **40**, 2847 (1989).

[4] F. Natterer, *The Mathematics of Computerized Tomography* (Wiley, New York, 1986).

[5] I. S. Gradshteyn and I. M. Ryzhik, *Table of Integrals, Series, and Products* (Academic, New York, 1980).

[6] G. M. D'Ariano and M. G. A. Paris, Phys. Rev. A **49**, 3022 (1994).

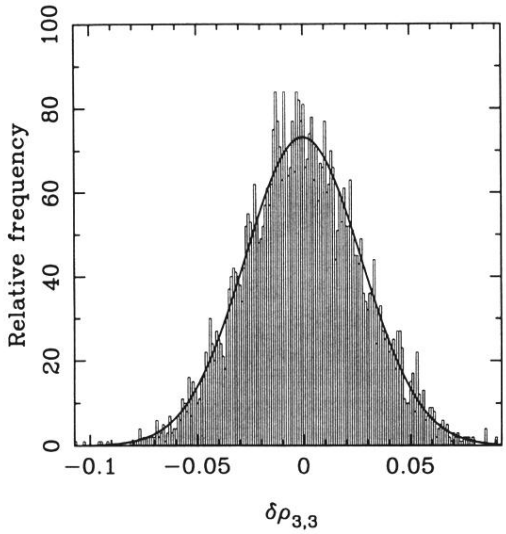

FIG. 1. Distribution of the tomographic outcomes for the matrix element $\rho_{3,3}$ (deviations $\delta\rho_{3,3}$ around the average). The computer-simulated experimental values are obtained for a coherent state with $\langle n \rangle = 3$. The histogram contains 5000 experiments (subensembles of data), each performed with $F = 27$ scanning phases and 100 measurements for each phase. The Gaussian curve with variance equal to the experimental rms error is superimposed.